THESIS FOR DEGREE OF LICENTIATE OF PHILOSOPHY

Diffusion-Induced Nonlinear Dynamics in Carbon Nanomechanical Resonators

CHRISTIN EDBLOM

Department of Applied Physics
CHALMERS UNIVERSITY OF TECHNOLOGY
Göteborg, Sweden 2015

Diffusion-Induced Nonlinear Dynamics in Carbon Nanomechanical Resonators
CHRISTIN EDBLOM

Department of Applied Physics
Chalmers University of Technology
SE-412 96 Göteborg, Sweden
Sweden
Telephone +46–(0)31–7721000

Typeset in LaTeX. Figures created using Matlab.

Chalmers reproservice
Göteborg, Sweden 2015

Diffusion-Induced Nonlinear Dynamics in Carbon Nanomechanical Resonators
CHRISTIN EDBLOM
Department of Applied Physics
Chalmers University of Technology

ABSTRACT

The emergence of nanoelectromechanical systems has enabled the development of sensors capable of detecting mass, charge, force, position, and spin with an unprecedented precision. In particular, the low mass, high resonant frequency, and high quality factor of carbon nanomechanical resonators make them ideal for the creation of a high sensitivity mass sensor. Carbon nanotube resonators are indeed the basis of the most sensitive mass sensors to date, whereas resonators made from suspended graphene monolayers are potentially capable of a very high rate of operation, due to their large surface area. A complicating factor is that the available mass measurement schemes rely on that the measured mass remains stationary, something that is no longer true at non-cryogenic temperatures.

In this thesis, the effect of an elevated ambient temperature on a mass-resonator system is studied by simulating ring-down experiments. Thermal fluctuations in the position of the mass on the resonator introduce a stochastic force in the system equations of motion; these stochastic differential equations are here solved analytically and numerically. The unperturbed resonator is modeled as an undamped linear oscillator, but the addition of a diffusing mass induces nonlinear dynamics in the system. The presence of the particle mediates a coupling between vibrational modes, that acts as a new dissipation channel. Additionally, short-time correlations between the motion of the diffusing particle and the vibrating resonator results in a second dissipation mechanism, that causes a nonexponential decay of the vibrational energy. For vibrational amplitudes that are much larger than the thermal energy this dissipation is linear; for small amplitudes the decay takes the same form as that of a nonlinearly damped oscillator.

KEYWORDS: nonequilibrium dynamics, nonlinear dynamics, noise, diffusion, dissipation, nanoelectromechanical systems, mass sensing, resonators, carbon nanotubes, graphene, stochastic differential equations, equations of motion, Fokker-Planck equation.

LIST OF PUBLICATIONS

This thesis consists of an introductory text and the following papers:

I **Diffusion-induced dissipation and mode coupling in nanomechanical resonators**
Christin Edblom and Andreas Isacsson
Physical Review B **90**, 155425 (2014)

Specification of my contribution to the publications

I I performed all the numerical calculations, and contributed to the analytical calculations as well as in writing the paper.

Contents

List of figures

1 Introduction

A factoid commonly quoted in high school math classes is that today's pocket-sized scientific calculators are smarter than early supercomputers, which filled entire rooms. Notwithstanding the accuracy of such a statement, it is indisputable that the ongoing miniaturization of components has been a crucial ingredient in the technological development of the last half-century. Fifty years ago, Gordon Moore noted that the number of components on a chip had doubled every two years for some time [1], and predicted that this trend would continue for at least another decade. With startling precision it has held true during five: a development driven by the decreased costs and increased operational speeds resulting from reduced system size.

The move towards smaller devices is not limited to integrated circuits; mechanical sensors like accelerometers and gyroscopes have been scaled down to micrometer-sized versions. Such microelectromechanical systems (MEMS) are today ubiquitous in modern cars, smartphones, and other consumer electronics. Even smaller sensors, nanoelectromechanical systems (NEMS), are the subject of much research motivated by their unprecedented sensitivity in measuring charge [2,3], force [4], position [5,6], spin [7], and mass [8–13]. It would be easy to conclude that smaller is always better, but is that really the case?

So far, the miniaturization of technology has largely been a matter of making smaller versions of existing mechanisms. However, since different physical processes will be relevant on microscopic length scales compared to those of our macroscopic day-to-day world [14], there is a limit to how small a replica of a device one can create without altering the manner in which it functions. Since atoms that make up the surface of a material do not always have the same properties as otherwise identical atoms deep in the bulk, and the surface-to-volume ratio of an object is inversely proportional to its linear size, surface effects will become progressively more important as devices are made smaller. Nano- to micrometersized systems can conduct charge and heat in unfamiliar ways, as their size can be comparable to the typical distance between particle collisions. Very small systems, consisting of a few atoms or molecules, will be governed by quantum mechanics; Heisenberg's uncertainty principle then places fundamental restrictions on how accurate measurements can become, as well as how small a volume one can confine particles to. Finally, and of interest to this thesis, small systems are subject to significant thermal fluctuations: random variations in, for example, particle positions and velocities that are due

to energy exchanged during unpredictable interactions with the environment.

The size of a system does not effect whether it interacts with its environment; thermal fluctuations in some form are always present. However, they remain negligible while the energy scale of the system dynamics (say, the vibrational energy of an oscillating beam) is much larger than the thermal energy contained in the environment. The former energy scale does depend on the size of a system, whereas the latter is a function only of temperature. Decreasing the system size while keeping the surrounding conditions unchanged will thus eventually render the two energy scales comparable. Consequently, at some point of miniaturization, the dynamics of a system will be considerably altered due to the presence of thermal fluctuations.

The particular realization of thermal fluctuations is system dependent; the underlying physical processes as well as in which quantities fluctuations will appear varies depending on the particular situation. For this reason, the discussion is henceforth restricted to the particular type of system that is the subject of this thesis. I will study a small particle stuck on the surface of a nanomechanical resonator* in the shape of a vibrating beam or drum; the resonator is on the order of 1 μm across.

1.1 Noise in a resonator-particle system

A solid can be thought of as a large number of atoms organized in a regular pattern: a lattice. A non-zero temperature will cause all these atoms to vibrate slightly around their equilibrium positions, in a chaotic manner. Then, a particle placed on the surface of this solid will be subject to a large number of small "kicks" from the vibrating atoms. Since the force imparted by each kick has an unpredictable direction and magnitude, the result is that the particle will bounce about on the surface in a random path. This is exactly what happens in a system consisting of a particle adsorbed on a resonator; the resonator atoms will vibrate, causing thermal fluctuations in the position of the particle.

Nanomechanical sensing schemes generally rely on monitoring how the resonant frequency of the resonator changes when the system is disturbed [15]. For example, mass can be measured by noting that if a particle of mass m is added to a resonator of mass M, the change $\Delta\omega < 0$ in the resonant frequency ω of the vibration mode ϕ is given by

$$-\frac{\Delta\omega}{\omega} \approx \tfrac{1}{2}\phi^2(x_\mathrm{p})\frac{m}{M}, \tag{1.1}$$

where x_p is the position of the added particle. It is thus clear that if there are

*In theoretical physics in general, an oscillator is any system that can be described by a Hamiltonian of the form $\mathcal{H} = \frac{1}{2m}p^2 + \frac{1}{2}m\omega^2x^2$. In the field of nanomechanics, however, we adopt terminology borrowed from engineering, in which only systems that by themselves *produce* an oscillatory signal are referred to as oscillators. Systems that require an external force to begin oscillating, like pendulums, springs and LC-circuits, are called resonators.

thermal fluctuations in x_p the frequency shift $\Delta\omega$ will also vary, introducing a source of noise in the measurement.

Typically, the vibration amplitude of a driven resonator as a function of the drive frequency is a Lorentzian, strongly peaked around the resonant frequency. If frequency fluctuations (also referred to as phase noise [16]) are present, this response curve changes. The peak broadens and can lose its symmetric shape, and may even develop a fine structure [17–20]. However, spectral broadening also results from the dissipation of energy, the mechanisms of which are not yet completely understood in NEMS [15, 21–23]. To further complicate the picture, carbon nanoresonators are nonlinear in many ways; nonlinear damping is present [24, 25], as well as an inherent, or geometric, nonlinearity that causes dissipation [26] and broadening [27]. In addition, diffusing adsorbates can induce a nonlinear response to driving [28,29], and they are also expected to cause dissipation and to enable different vibrational modes to interact. Clearly, there are several mechanisms present in nanoelectromechanical resonators that can manifest in similar ways, and that interact in a non-trivial manner.

Here, I attempt to shed some light on this situation by studying the dynamics caused by a diffusing particle adsorbed on a resonator. To eliminate all complications related to the forced response of a resonator, only its ring-down is studied: simulated measurements similar to those of recent experiments [30,31]. In addition, I make use of a theoretician's privileged situation and exclude from the model all damping mechanisms except for the one associated with the diffusing particle according to the fluctuation-dissipation theorem. What remains is a perfectly linear, undamped resonator that, once excited, would oscillate in the same fashion forever. Any deviation from this behaviour is thus attributable to the presence of the adsorbed diffusing particle. The goal of the study is to verify whether diffusion does indeed induce damping and mode coupling, and if that is the case, to examine the resulting system dynamics.

1.2 Thesis outline

In attempting to describe something complicated, it can be a productive strategy to break the problem down into smaller, and hopefully easier, parts. Here, I shall endeavour to do just that. I begin in chapter 2 by studying the dynamics of a nanoresonator without an adsorbed particle, and continue in chapter 3 by examining the random motion of a particle on an immobile substrate. The two parts are connected in chapter 4, in which I discuss the nonlinear dynamics induced by the diffusing particle. The thesis concludes with a summary in chapter 5, alongside an outlook on future work.

2 Dynamics of nanomechanical resonators

In this chapter, I describe a resonator in an unperturbed state: before any extra particles are added. I do this by writing down the Lagrangian density [32] of the resonator, determined from elasticity theory [33]. From this Lagrangian I then find the resonator equations of motion, which are solved for the vibrational eigenmodes and corresponding frequencies.

It may seem surprising that a *nano*mechanical resonator can be modelled accurately by continuum mechanics, a classical theory that is successfully applied to the steel beams making up our bridges and buildings; beams that are many orders of magnitude larger than a nanomechanical resonator. The key is that continuum mechanics is a theory of deformations, and will perform very well as long as the length scale of these deformations is much larger than the length scale of any inhomogeneities in the solid being deformed. In the case of a carbon resonator, the length scale for inhomogeneities is the typical distance between atoms in the material: 10-20 Å. The characteristic length scale for a deformation is the wave length of a vibrational mode. As I show in this chapter, such wave lengths are on the order of the size of the resonator: four orders of magnitude larger than the interatomic distance. This separation of length scales is more than enough to consider the resonator as a smooth, homogeneous solid, and continuum mechanics is then an appropriate theory to use.

2.1 Lagrangian density

A deformed elastic body is characterized by the displacement field $\mathbf{u}(\mathbf{x},t) = (u_1(x_1,x_2,x_3,t), u_2(x_1,x_2,x_3,t), u_3(x_1,x_2,x_3,t))$. That is, an infinitesimal volume element which in the relaxed solid is centered at $\mathbf{x} = (x_1,x_2,x_3)$ will, under deformation, be moved to the position $\mathbf{x}+\mathbf{u}(\mathbf{x},t)$. Such a deformation introduces a strain in the solid, described by the strain tensor $\boldsymbol{\varepsilon}$ [33], whose elements are

$$\varepsilon_{ij} = \frac{1}{2}\left(\frac{\partial u_i}{\partial x_j} + \frac{\partial u_j}{\partial x_i} + \sum_k \frac{\partial u_k}{\partial x_i}\frac{\partial u_k}{\partial x_j}\right). \tag{2.1}$$

The potential energy stored in a deformed body is given by the stretching free energy density:

$$\mathcal{F}_S = \sum_{i,j} \left[\tfrac{1}{2}\lambda \varepsilon_{ii}\varepsilon_{jj} + \mu \varepsilon_{ij}\varepsilon_{ij} \right]. \tag{2.2}$$

where the Lamé parameters μ and λ quantify the shear and compressive strain, respectively.

In addition to the stretching energy density, there is a free energy density associated with bending without stretching; in a body with bending rigidity κ it is

$$\mathcal{F}_B = \tfrac{1}{2}\kappa \sum_i \left| \sum_j \frac{\partial^2 u_i}{\partial x_j^2} \right|^2. \tag{2.3}$$

Finally, the strain tensor $\boldsymbol{\varepsilon}$ is related to the stress tensor $\boldsymbol{\sigma}$ through the general Hooke's law:

$$\boldsymbol{\sigma} = 2\mu\boldsymbol{\varepsilon} + \lambda \operatorname{Tr}[\boldsymbol{\varepsilon}]\, \mathbf{I}, \tag{2.4}$$

where $\mathbf{I}$ is an identity matrix.

In this thesis, I am concerned with resonators that can be described as one- and two-dimensional, henceforth referred to as beams and membranes. The latter case is experimentally realized in resonators created by atomically thin membranes, like graphene [24–26, 34–37]. A resonator that acts one-dimensional is achieved by using a solid whose length is several orders of magnitude larger than its width and depth. A prime example of such a device is a carbon nanotube (CNT) resonator [10, 24, 27, 38–41].

In the following, I set $\mathbf{x} = (x, y)$ in order to describe a two-dimensional resonator. The one-dimensional case will, in the final expressions (2.8) and (2.10), be easily found by replacing gradients with one-dimensional spatial derivatives. In addition, I only consider flexural (out-of-plane) displacements. This is an adiabatic approximation based on the rate of change of the respective displacements; the characteristic frequencies for the flexural oscillation of a nanoresonator are much lower than the frequencies of longitudinal vibration. Thus, for any deformation, the in-plane displacement field relaxes into a static state before the flexural displacement shows any discernible change. With regards to the resonator dynamics, then, the displacement field may be approximated [42] as $\mathbf{u}(\mathbf{x}, t) = (0, 0, u_3(\mathbf{x}, t))$. I redefine $u_3(\mathbf{x}, t) = w(x, y, t)$, and find that the strain tensor simplifies to

$$\boldsymbol{\varepsilon} = \frac{1}{2}\begin{pmatrix} (\partial_x w)^2 & \partial_x w \partial_y w \\ \partial_x w \partial_y w & (\partial_y w)^2 \end{pmatrix} = \tfrac{1}{2}\nabla w (\nabla w)^T. \tag{2.5}$$

Here, $\partial_x w \equiv \partial w / \partial x$, and the gradient ∇ is defined as a column vector.

Under the given conditions (that, in particular, ensure that $\varepsilon_{xy}^2 = \varepsilon_{xx}\varepsilon_{yy}$), the stretching free energy density can be written

$$\mathcal{F}_S = \tfrac{1}{2} \operatorname{Tr}[\boldsymbol{\sigma}] \operatorname{Tr}[\boldsymbol{\varepsilon}] = \tfrac{1}{2} \operatorname{Tr}[\boldsymbol{\sigma}] [\nabla w \cdot \nabla w]. \tag{2.6}$$

Henceforth it is assumed that $\mathrm{Tr}\,[\boldsymbol{\sigma}] \equiv \sigma = \textit{constant}$, an assumption that is valid for the resonators under discussion if the vibration amplitude is small or if there is a large prestrain present, for example due to the fabrication process.

The bending free energy density becomes

$$\mathcal{F}_B = \tfrac{1}{2}\kappa \left[\nabla^2 w\right]^2. \tag{2.7}$$

Introducing the mass density ρ, I thus conclude that the Lagrangian density of a one- or twodimensional body that is deformed only in the flexural direction is

$$\mathcal{L}_0 = \tfrac{1}{2}\rho\dot{w}^2 - \tfrac{1}{2}\sigma\left[\nabla w \cdot \nabla w\right] - \tfrac{1}{2}\kappa\left[\nabla^2 w\right]^2 \tag{2.8}$$

2.2 Equations of motion

By setting the variation of the action S caused by (2.8) to zero, the equations of motion are found. That is,

$$\begin{aligned} 0 = \delta S &= \delta \int \mathrm{d}\mathbf{x}\mathrm{d}t\ \mathcal{L}_0 = \\ &= \int \mathrm{d}\mathbf{x}\mathrm{d}t \left(\rho\dot{w}\delta\dot{w} - \sigma\nabla w \cdot \delta(\nabla w) - \kappa\nabla^2 w\delta(\nabla^2 w)\right) \\ &= \int \mathrm{d}\mathbf{x}\mathrm{d}t \left(-\rho\ddot{w} + \sigma\nabla^2 w - \kappa\nabla^4 w\right)\delta w. \end{aligned} \tag{2.9}$$

In the final step, a number of partial integrations were performed. I consider resonators with clamped boundaries, on which $\delta w = 0, \delta(\nabla w) = 0$; the boundary terms in the partial integrations consequently vanish. Finally, since the variation δw is arbitrary, the equality (2.9) will only hold if the bracketed term is zero:

$$\rho\ddot{w} - \sigma\nabla^2 w + \kappa\nabla^4 w = 0. \tag{2.10}$$

This is the equation of motion for the flexural displacement field of a resonator.

Without loss of generality, the displacement $w(\mathbf{x}, t)$ can be written as a sum of resonator eigenmodes:

$$w(\mathbf{x}, t) = \sum_{n=0}^{\infty} q_n(t)\varphi_n(\mathbf{x}), \tag{2.11}$$

where

$$-\omega_n^2\rho\varphi_n - \sigma\nabla^2\varphi_n + \kappa\nabla^4\varphi_n = 0. \tag{2.12}$$

Here, ω_n is the frequency of the vibration mode $\varphi_n(\mathbf{x})$. I shall now explicitly determine the eigenfrequecies and -modes for the the geometries under discussion.

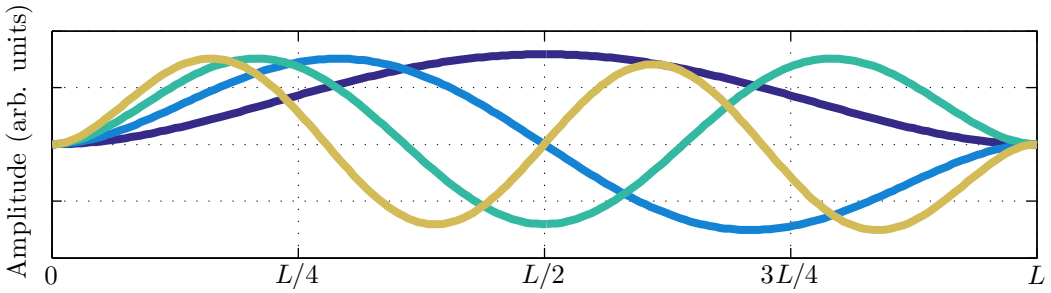

Figure 2.1: Vibrational eigenmodes of a doubly clamped beam of length L.

2.2.1 Beam eigenmodes

I consider a one-dimensional resonator of length L that is doubly clamped: $\varphi_n(0) = \varphi_n(L) = \varphi_n'(0) = \varphi_n'(L) = 0$. The now-ordinary differential equation (2.12) has the characteristic equation

$$\kappa k^4 - \sigma k^2 - \rho\omega_n^2 = 0, \tag{2.13}$$

with roots $\pm k_n^+, \pm i k_n^-$, where

$$k_n^\pm = \sqrt{\sqrt{\frac{\sigma^2}{4\kappa^2} + \frac{\rho\omega_n^2}{\kappa}} \pm \frac{\sigma}{2\kappa}}. \tag{2.14}$$

The general solution for the eigenfunction $\varphi_n(x)$ is thus

$$\varphi_n(x) = A_n \sinh k_n^+ x + A_n' \sin k_n^- x + B_n \cosh k_n^+ x + B_n' \cos k_n^- x, \tag{2.15}$$

where the integration constants will be chosen so that the φ_n are real and normalized to L:

$$\int_0^L \mathrm{d}x\ \varphi_m(x)\varphi_n(x) = L\delta_{mn}. \tag{2.16}$$

That the eigenfunctions are orthogonal is straight-forwardly verified; see for example [43].

The algebra involved in determining the $A_n^{(\prime)}, B_n^{(\prime)}$ and the eigenfrequencies ω_n turns out to be simplified by a change of variables to $\Xi = x - L/2$. Then, the boundary conditions neatly divide the φ_n into sets of even and odd functions:

$$\begin{aligned}\varphi_{2n}(\Xi) &= A_{2n} \cosh k_{2n}^+ \Xi + A_{2n}' \cos k_{2n}^- \Xi \\ \varphi_{2n+1}(\Xi) &= B_{2n+1} \sinh k_{2n+1}^+ \Xi + B_{2n+1}' \sin k_{2n+1}^- \Xi.\end{aligned} \tag{2.17}$$

The eigenfrequencies ω_n are determined from the equation

$$\frac{k_n^\mp}{k_n^\pm} = \pm \frac{\tan k_n^- \frac{L}{2}}{\tanh k_n^+ \frac{L}{2}}, \tag{2.18}$$

Table 2.1: Normalized eigenfrequency ω_n/ω_0 for the n:th excited mode of a beam and a membrane resonator, where ω_0 is the fundamental mode frequency (corresponding to $(\mu,\nu) = (0,1)$ for the membrane). For the beam resonator, a good approximation for the ratio ω_n/ω_0 is $\frac{1}{9}(2n+1)^2$, while for the membrane $\omega_n/\omega_0 \approx \frac{6}{5}\sqrt{n}$. Note also the two-fold degeneracy of many of the membrane excited modes.

n	Beam	Membrane	(μ,ν)
1	2.7245	1.5933	$(\pm1,1)$
2	5.3139	2.1355	$(\pm2,1)$
3	8.7633	2.2954	$(0,2)$
4	13.074	2.6531	$(\pm3,1)$
5	18.246	2.9173	$(\pm1,2)$
6	24.280	3.1555	$(\pm4,1)$
7	31.176	3.5001	$(\pm2,2)$

where upper (lower) signs correspond to odd (even) n. While the value of the frequencies depend on material parameters, the ratio between them is only a function of the resonator geometry. Table 2.1 lists the ratio ω_n/ω_0 for some excited modes: ω_0 denotes the fundamental mode frequency. A quick estimate is given by $\omega_n/\omega_0 \approx \frac{1}{9}(2n+1)^2$

Finally, the integration constants $A_n^{(\prime)}$ and $B_n^{(\prime)}$ are found from the boundary conditions combined with the normalization chosen in (2.16). The result is that

$$A'_n = -\frac{\cosh k_n^+ \frac{L}{2}}{\cos k_n^- \frac{L}{2}} A_n, \quad B'_n = -\frac{\sinh k_n^+ \frac{L}{2}}{\sin k_n^- \frac{L}{2}} B_n \tag{2.19}$$

and

$$\begin{aligned} |A_n|^2 &= 2\left[1 + \frac{\sinh k_n^+ L}{k_n^+ L} + \frac{\cosh^2 k_n^+ \frac{L}{2}}{\cos^2 k_n^- \frac{L}{2}}\left(1 + \frac{\sin k_n^- L}{k_n^- L}\right)\right]^{-1}, \\ |B_n|^2 &= 2\left[1 - \frac{\sinh k_n^+ L}{k_n^+ L} - \frac{\sinh^2 k_n^+ \frac{L}{2}}{\sin^2 k_n^- \frac{L}{2}}\left(1 - \frac{\sin k_n^- L}{k_n^- L}\right)\right]^{-1}. \end{aligned} \tag{2.20}$$

The final undetermined phase is chosen so that the φ_n are real.

While the expressions for the eigenmodes may look complicated, the mode shapes can be thought of as sines and cosines that have been somewhat deformed in order to fit the doubly clamped boundary conditions. The four lowest vibrational modes are shown in figure 2.1 (page 8).

2.2.2 Membrane eigenmodes

For an atomically thin graphene membrane [44], the bending rigidity κ is very small [45], and may be neglected. Then, (2.12) becomes the Helmholtz equation

$$\nabla^2 \varphi_n = -\frac{\omega_n^2 \rho}{\sigma} \varphi_n, \tag{2.21}$$

with the known [46] solutions

$$\varphi_n(r,\theta) = A_n e^{i\mu\theta} J_{|\mu|}\left(\omega_n \sqrt{\frac{\rho}{\sigma}} r\right). \tag{2.22}$$

Here, $\mu \in \mathbb{Z}$ and J_μ is a Bessel function of the first kind. All eigenmodes with $\mu \neq 0$ are doubly degenerate.

The boundary condition that $\varphi_n(R,\theta) = 0$ fixes the eigenfrequencies as

$$\omega_n = \frac{\alpha_{|\mu|\nu}}{R} \sqrt{\frac{\sigma}{\rho}}, \tag{2.23}$$

where $\alpha_{\mu\nu}$ is the ν:th zero of J_μ. The index n must now be interpreted as a vector index $n = (\mu, \nu)$. Again, the ratio between eigenfrequencies depends only on the resonator geometry: some of the normalized excited mode frequencies are listed in table 2.1. A quick estimate of the frequency ratio is $\omega_n/\omega_0 \approx \frac{6}{5}\sqrt{n}$.

The eigenfunctions are orthogonal by construction, and the normalization is chosen so that

$$\int_0^{2\pi} \mathrm{d}\theta \int_0^R r\mathrm{d}r \; \varphi_n^*(r,\theta)\varphi_m(r,\theta) = \pi R^2 \delta_{mn} \tag{2.24}$$

by setting

$$A_n = \left[J_{|\mu|+1}\left(\omega_n \sqrt{\frac{\rho}{\sigma}} R\right)\right]^{-1} = \left[J_{|\mu|+1}\left(\alpha_{|\mu|\nu}\right)\right]^{-1}. \tag{2.25}$$

The shape of the four lowest vibrational modes is shown in figure 2.2 (page 11).

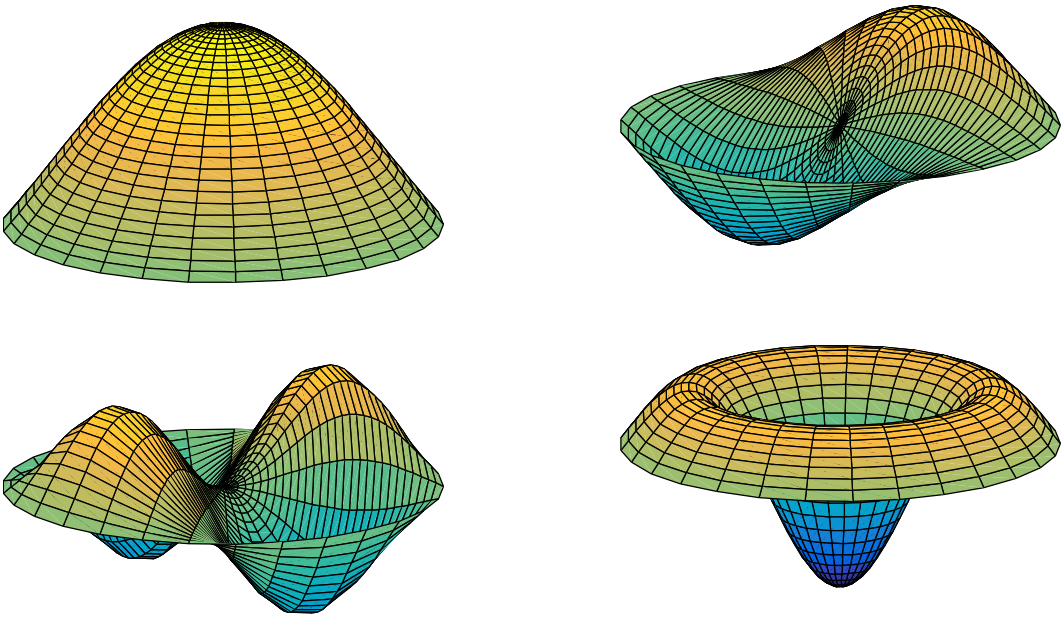

Figure 2.2: Vibrational eigenmodes of a circular membrane. Those excited modes that are not rotationally symmetric are degenerate; there is a second eigenmode with the same frequency but with a phase difference of $\pi/2$.

3 Particle diffusion

In chapter 2, I described the unperturbed resonator, without the added complication of an adsorbed particle. Here, I will approach the problem from the opposite direction, and describe the motion of a particle over the surface of a solid, without the added complication of allowing this solid to move.

I mentioned in section 1.1 that a particle adsorbed on a solid is, at any given time, subject to a large number of random "kicks" caused by lattice vibrations in the substrate. As a result, the particle will perform a random walk over the surface of the solid, a random walk that is now mathematically characterized.

3.1 The Langevin equation

The position* x of a particle of mass m is described by Newton's second law,

$$m\ddot{x} = F(t). \tag{3.1}$$

In the present case, $F(t)$ is the sum of all forces exerted by the lattice vibrations on the particle. There will be two qualitatively different contributions to this force: one stochastic (random) and one dissipative.

I shall assume that the stochastic component of $F(t)$ is normally distributed. This is based on that the force is the sum of a large number of random variables (the vibrations of each lattice atom) and will thus tend to a normal distribution according to the central limit theorem [47]. Then, the stochastic force can be written as $\sigma\xi(t)$, where σ is its standard deviation and $\xi(t) \in \mathcal{N}[0,1]$. Furthermore, I make the physically reasonable assumptions that if the particle is stationary it will, on average, be kicked equally often in every direction, and that since lattice vibrations are random, the net direction of the kicks at time t will not have any influence on the net direction at another time t'. Formally, this translates to that the mean $\langle\xi(t)\rangle = 0$, and that $\xi(t)$ is a white noise process with correlation function $\langle\xi(t)\xi(t')\rangle = \delta(t-t')$.

If, on the other hand, the particle is moving, it will be "in range" of the lattice vibrations of a larger number of substrate atoms, in particular along

*For convenience, x is written as a scalar in this chapter. For $x \in \mathbb{R}^n$, the force $F(t)$ also becomes an n-dimensional vector, and there will be n copies of equation (3.1): one for each component of x.

the direction of motion. Consequently, the particle will meet more kicks along that direction. The net effect of this increased collision rate γ is a friction force between the particle and the substrate, that increases if the particle moves faster. This dissipative contribution to $F(t)$ is modelled as $-m\gamma\dot{x}$. Thus, equation (3.1) can be written[†]

$$m\ddot{x} + m\gamma\dot{x} = \sigma\xi(t). \tag{3.2}$$

This is the Langevin equation [50]. In figure 3.1 a), I show two paths found by solving equation (3.2) in one dimension, with reflecting boundary conditions. Both paths begin at the same position.

The fact that random forces (the $\sigma\xi(t)$ in equation (3.2)) always[‡] occur together with friction (the $m\gamma\dot{x}$) is a reflection of the fluctuation-dissipation theorem (FDT) [47]. The FDT is also seen in the fact that the standard deviation σ of the stochastic force is related to the damping: $\sigma = \sqrt{2m\gamma k_{\mathrm{B}}T}$. This expression is found by formally integrating equation (3.2) to find the velocity

$$\dot{x} = v_0 e^{-\gamma t} + \frac{\sigma}{m}\int_0^t \mathrm{d}t'\; e^{-\gamma(t-t')}\xi(t'), \tag{3.3}$$

where v_0 is given by the initial conditions. Equation (3.3) is then substituted in the equipartition theorem $\frac{1}{2}k_{\mathrm{B}}T = \frac{1}{2}m\left\langle\dot{x}\right\rangle^2$, which can be simplified using the properties of the stochastic process $\xi(t)$ and taking a $t \to \infty$-limit.

Finally, it will be of interest to study the overdamped limit of the Langevin equation. In this limit, the damping rate γ is large enough that $\ddot{x} \ll \gamma\dot{x}$, and equation (3.2) becomes

$$\dot{x} = \frac{\sigma}{m\gamma}\xi(t) = \sqrt{\frac{2k_{\mathrm{B}}T}{m\gamma}}\xi(t) \equiv \sqrt{2D}\;\xi(t). \tag{3.4}$$

In the final step the diffusion constant D is defined; this is the same diffusion constant as the one appearing in the diffusion equation $\dot{\mathcal{U}} = D\partial_x^2\mathcal{U}$, where $\mathcal{U}$ is the density field of some diffusing quantity [46]. The reason for this is made clear in the next section.

[†]A much more careful derivation is certainly possible, for example from the Caldeira-Leggett model [48]. To read this thesis, however, an intuitive understanding of the Langevin equation is sufficient. The presented phenomenological argument is adapted from [49].

[‡]The FDT is valid as long as the system in question obeys detailed balance [47]. In our case, the principle of detailed balance can be formulated as $p(x_A)w_{A\to B} = p(x_B)w_{B\to A}$. Here, $p(x_A)$ is the probability that the particle is found at position x_A and $w_{A\to B}$ is the probability that the particle will move from x_A to x_B. The equation of detailed balance thus expresses that, over time, the particle will move from x_A to x_B (a transition that, of course, requires that the particle is present at x_A to begin with) as often as it will move from x_B to x_A.

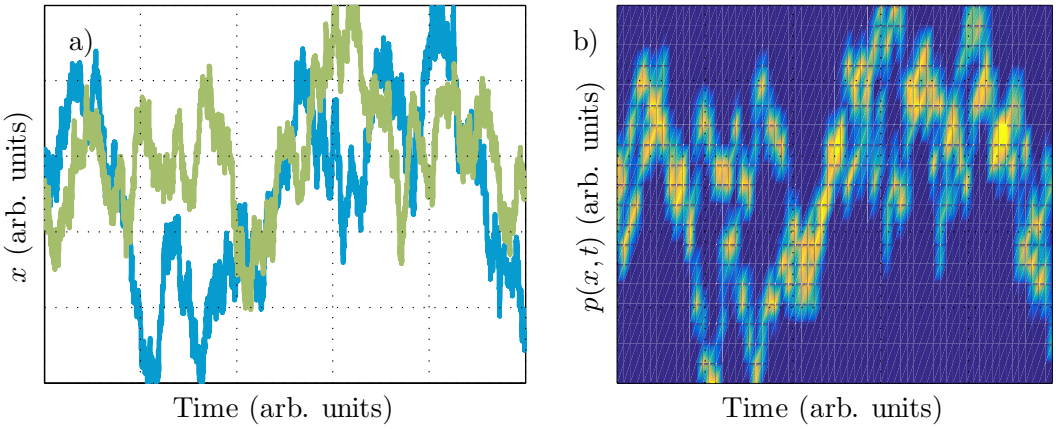

Figure 3.1: a) Two example paths of a particle performing a random walk in one dimension with reflecting boundary conditions. Both paths begin at the same position. b) Probability distribution $p(x,t)$ for the particle position based on the two trajectories in a). Dark (light) areas indicate positions where the probability to find the particle is small (large).

3.2 The Fokker-Planck equation

The Langevin equation (3.2) expresses the system dynamics directly in terms of the fluctuating variable x. Another way to deal with stochastic quantities is to work with their probability distribution $p(x,\dot{x},t)$. In terms of this distribution, one can calculate the probability that a particle under the influence of a stochastic force will be at[§] position x and have velocity $\dot{x}$ at time t as

$$P(x,\dot{x},t) = \int_x^{x+\mathrm{d}x} \mathrm{d}x' \int_{\dot{x}}^{\dot{x}+\mathrm{d}\dot{x}} \mathrm{d}\dot{x}'\; p\left(x',\dot{x}',t\right). \tag{3.5}$$

A partial differential equation determining the time evolution of a probability distribution is a Fokker-Planck equation (FPE).

Every stochastic differential equation (SDE) of the type

$$\frac{\partial \mathbf{x}}{\partial t} = \mathbf{A}(\mathbf{x},t) + \mathbb{B}(\mathbf{x},t)\boldsymbol{\xi}(t), \tag{3.6}$$

that describes the evolution of a random variable $\mathbf{x}$ subject to the drift $\mathbf{A}(\mathbf{x},t)$ and the diffusion process $\mathbb{B}(\mathbf{x},t)\boldsymbol{\xi}(t)$, has an equivalent FPE for the probability distribution of the random variable. If (3.6) is assumed to be a Stratonovich

[§]Used in the physicist's sense of "in a sufficiently small interval around".

SDE, this equivalent FPE is given by [47]

$$\frac{\partial p}{\partial t} = -\sum_i \frac{\partial}{\partial x_i}\big[A_i(\mathbf{x},t)p(\mathbf{x},t)\big] + \frac{1}{2}\sum_{i,j,k}\frac{\partial}{\partial x_i}\left[B_{ik}(\mathbf{x},t)\frac{\partial}{\partial x_j}\big[B_{jk}(\mathbf{x},t)p(\mathbf{x},t)\big]\right]. \tag{3.7}$$

As an illustrative example, I will here sketch a derivation of the FPE for the over-damped Langevin particle described by equation (3.4). I have chosen to use a transparent derivation that clearly shows the connection between the random variable and its probability distribution. However, it should be pointed out that it is a second order-calculation that "happens to be correct". This lucky coincidence is due to that the starting equation (3.4) is linear, and that the stochastic process is Gaussian with vanishing higher moments.

Since the particle in question must remain somewhere in space, the total probability is conserved. Hence, the probability distribution must obey the continuity equation:

$$\dot{p}(x,\dot{x},t) + \partial_x[\dot{x}p(x,\dot{x},t)] + \partial_{\dot{x}}[\ddot{x}p(x,\dot{x},t)] = 0. \tag{3.8}$$

If I naïvely use equation (3.4) to set $\ddot{x} = 0, \dot{x} = \sqrt{2D}\ \xi(t)$, (3.8) becomes

$$\dot{p} = -\sqrt{2D}\ \xi(t)\partial_x p. \tag{3.9}$$

This is not strictly accurate, since the probability distribution p represents a quantity related to the ensemble of realizations of $\xi(t)$, not a single trajectory of the force. However, after taking the ensemble average below, the end result will be correct.

Equation (3.9) is integrated from the time t to $t + \Delta t$:

$$p(t+\Delta t) = p(t) - \sqrt{2D}\int_t^{t+\Delta t} \mathrm{d}t'\ \xi(t')\partial_x p(t'). \tag{3.10}$$

For brevity, only the time dependence of $p(x,\dot{x},t)$ is explicitly shown. Equation (3.10) is substituted into itself[¶], and subsequently averaged over all realizations of the stochastic force $\xi(t)$:

$$\begin{aligned} p(t+\Delta t) &= p(t) - \left\langle \sqrt{2D}\int_t^{t+\Delta t} \mathrm{d}t'\ \xi(t')\partial_x\left[p(t) - \sqrt{2D}\int_t^{t'} \mathrm{d}t''\ \xi(t'')\partial_x p(t'')\right]\right\rangle \\ &= p(t) + 2D\int_t^{t+\Delta t}\mathrm{d}t'\int_t^{t'}\mathrm{d}t''\delta(t'-t'')\partial_x^2 p(t'') \end{aligned} \tag{3.11}$$

where I used that $\langle\xi(t)\rangle = 0$ and $\langle\xi(t)\xi(t')\rangle = \delta(t-t')$. Performing the final integrations, and assuming that Δt is sufficiently small that p stays constant

[¶]In this case, it is sufficient to take this iterative process only to the second order, since $\xi(t)$ is normally distributed. In general, one must study the limit of infinite iterations.

over the interval, yields

$$p(t + \Delta t) = p(t) + \Delta t D \partial_x^2 p(t). \tag{3.12}$$

The factor $\frac{1}{2}$ arises by considering the $\delta(t' - t'')$ as the limit of a sequence of progressively more peaked functions symmetric around the point $t'' = t'$, and noting that the integral only goes to the peak — only over half of the area bounded by the function curve. Rearranging terms and letting $\Delta t \to 0$ does indeed leave the diffusion equation

$$\dot{p} = D \frac{\partial^2 p}{\partial x^2}, \tag{3.13}$$

as expected from section 3.1.

In figure 3.1 b) is plotted the probability density for a variable that only has two realizations of the force $\xi(t)$, giving the two random walks shown in a). While such a force is not very common, figure 3.1 gives an intuitive sense of how the particle paths and the probability distribution is related. In a more realistic case, $\xi(t)$ would cause a very large number of possible paths, and the probability distribution would be constant; at any given time it would be equally probable to find the particle at any point of the domain.

4 Complete system

In this chapter, I will join the theory of chapters 2 and 3 in order to describe the combined system, where a particle is adsorbed on and allowed to diffuse across the surface of a resonator during its ringdown. The prototype systems under consideration are illustrated in figure 4.1 (page 20). I consider reflecting boundaries and zero desorbation probability; the particle will never leave the surface of the resonator.

4.1 Coupled equations of motion

Deriving the equations of motion is a three-step process. First, the Lagrangian density for the full system is written down and varied. The resulting equations of motion will be in terms of the displacement field and the particle position $\mathbf{x}_\mathrm{p}$, so the second step is to expand $w(\mathbf{x}, t)$ in a sum of eigenmodes according to equation (2.11). In the third and final step, a stochastic force and accompanying friction term are added by hand in the equation for $\mathbf{x}_\mathrm{p}$, motivated by the discussion in section 3.1.

Consider a particle of mass m that is adsorbed at position $\mathbf{x}_\mathrm{p}$ on the resonator surface; its position vector is then $\mathbf{r}(t) = (\mathbf{x}_\mathrm{p}(t), w(\mathbf{x}_\mathrm{p}(t), t))$. The Lagrangian density for the entire system is found by adding the kinetic energy of the adsorbed particle, $\frac{1}{2}m\dot{\mathbf{r}}^2$, to the resonator Lagrangian $\mathcal{L}_0$, equation (2.8). That is,

$$\mathcal{L} = \mathcal{L}_0 + \tfrac{1}{2}m\delta(\mathbf{x}_\mathrm{p} - \mathbf{x}) \left[\dot{\mathbf{x}}_\mathrm{p}^2 + \left(\dot{w}(\mathbf{x}_\mathrm{p}, t) + \dot{\mathbf{x}}_\mathrm{p} \cdot \nabla w(\mathbf{x}_\mathrm{p}, t)\right)^2\right]. \tag{4.1}$$

The $\delta(\mathbf{x}_\mathrm{p} - \mathbf{x})$ ensures that the particle is point-like.

The variation of the field w now yields

$$\begin{aligned} 0 = \delta S &= \delta \int \mathrm{d}\mathbf{x}\mathrm{d}t\ \mathcal{L} = \\ &= \int \mathrm{d}\mathbf{x}\mathrm{d}t\ \left[\delta\mathcal{L}_0 + m\delta(\mathbf{x}_\mathrm{p} - \mathbf{x})(\dot{w} + \dot{\mathbf{x}}_\mathrm{p} \cdot \nabla w)\left(\delta\dot{w} + \dot{\mathbf{x}}_\mathrm{p} \cdot \delta(\nabla w)\right)\right]. \end{aligned} \tag{4.2}$$

Note that $\dot{w} + \dot{\mathbf{x}}_\mathrm{p} \cdot \nabla w = \frac{\mathrm{d}}{\mathrm{d}t} w(\mathbf{x}_\mathrm{p}(t), t) \equiv \dot{w}_\mathrm{p}$. The new term in $\mathcal{L}$ is partially integrated, and as in the unperturbed case $\delta w = 0$ on the boundary, due to

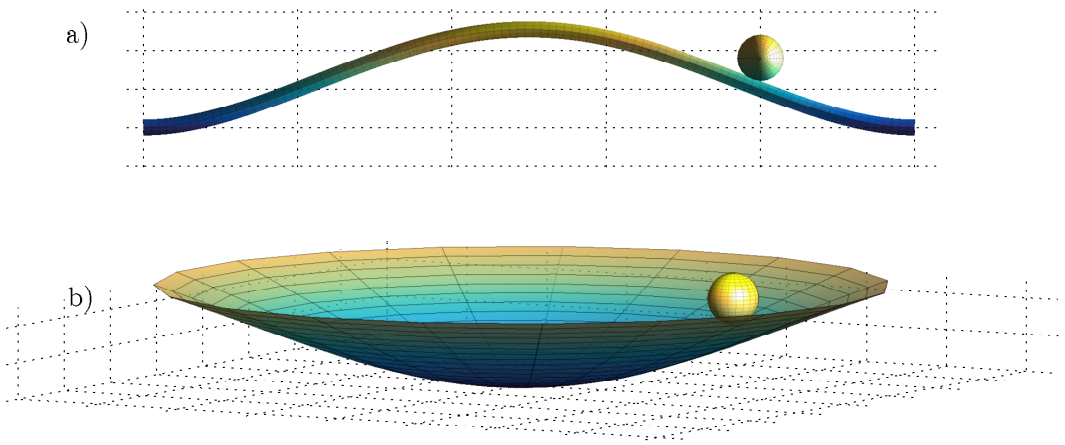

Figure 4.1: The systems under discussion in this thesis: a particle adsorbed on the surface of NEMS resonator in the shape of a) a doubly clamped beam or b) a circular membrane with a pinned boundary.

clamped resonator edges. The result is

$$0 = \int \mathrm{d}\mathbf{x}\mathrm{d}t \ \left[\delta\mathcal{L}_0 - \delta w \left[\frac{\partial}{\partial t} + \dot{\mathbf{x}}_\mathrm{p}\cdot\nabla\right]\left(m\delta(\mathbf{x}_\mathrm{p}-\mathbf{x})\dot{w}_\mathrm{p}\right)\right]. \tag{4.3}$$

The term resulting from the derivatives acting on the $\delta(\mathbf{x}_\mathrm{p}-\mathbf{x})$ will cancel, resulting in the equation of motion

$$\rho\ddot{w} - \sigma\nabla^2 w + \kappa\nabla^4 w + m\delta(\mathbf{x}_\mathrm{p}-\mathbf{x})\ddot{w}_\mathrm{p} = 0, \tag{4.4}$$

where $\ddot{w}_\mathrm{p} \equiv \frac{\mathrm{d}^2}{\mathrm{d}t^2} w(\mathbf{x}_\mathrm{p}(t),t)$.

Varying $\mathbf{x}_\mathrm{p}$ instead results in

$$\begin{aligned} 0 = \delta S &= \delta \int \mathrm{d}\mathbf{x}\mathrm{d}t \ \tfrac{1}{2}m\delta(\mathbf{x}_\mathrm{p}-\mathbf{x})\left[\dot{\mathbf{x}}_\mathrm{p}^2 + (\dot{w}(\mathbf{x}_\mathrm{p},t) + \dot{\mathbf{x}}_\mathrm{p}\cdot\nabla w(\mathbf{x}_\mathrm{p},t))^2\right] \\ &= \delta \int \mathrm{d}t \ \tfrac{1}{2}m\left[\dot{\mathbf{x}}_\mathrm{p}^2 + (\dot{w}(\mathbf{x}_\mathrm{p},t) + \dot{\mathbf{x}}_\mathrm{p}\cdot\nabla w(\mathbf{x}_\mathrm{p},t))^2\right] \\ &= m\int \mathrm{d}t \left[\dot{\mathbf{x}}_\mathrm{p}\cdot\delta\dot{\mathbf{x}}_\mathrm{p} + \dot{w}_\mathrm{p}\left(\nabla\dot{w}\cdot\delta\mathbf{x}_\mathrm{p} + \delta\dot{\mathbf{x}}_\mathrm{p}\cdot\nabla w + \dot{\mathbf{x}}_\mathrm{p}\cdot\delta\mathbf{x}_\mathrm{p}\nabla^2 w\right)\right]. \end{aligned} \tag{4.5}$$

The required partial integrations are performed, leaving the equation of motion

$$m\ddot{\mathbf{x}}_\mathrm{p} + m\ddot{w}_\mathrm{p}\nabla w(\mathbf{x}_\mathrm{p},t) = 0. \tag{4.6}$$

Equations (4.4) and (4.6) determine the dynamics of the resonator-particle system in the absence of thermal fluctuations.

The displacement field is now expanded as a sum of eigenmodes:

$$w(\mathbf{x},t) = \sum_k q_k(t)\varphi_k(\mathbf{x}). \tag{4.7}$$

The mode functions $\varphi_k(\mathbf{x})$ are given by equation (2.17) for the beam and by equation (2.22) for the membrane. In order to obtain an equation for the mode amplitudes $q_k(t)$, I use that the eigenmodes are solutions of the unperturbed equation of motion: $-\sigma\nabla^2\varphi_k(\mathbf{x}) + \kappa\nabla^4\varphi_k(\mathbf{x}) = \rho\omega_k^2\varphi_k(\mathbf{x})$. The factor $\ddot{w}_\mathrm{p}$ is only present in perturbative terms, so it may be approximated as

$$\ddot{w}_\mathrm{p} = \frac{\mathrm{d}^2}{\mathrm{d}t^2}w(\mathbf{x}_\mathrm{p}(t),t) = \frac{\mathrm{d}^2}{\mathrm{d}t^2}\sum_k q_k(t)\varphi_k(\mathbf{x}_\mathrm{p}) \approx -\sum_k \omega_k^2 q_k(t)\varphi_k(\mathbf{x}_\mathrm{p}). \tag{4.8}$$

Finally, the inner product of equation (4.4) with $\varphi_n(\mathbf{x})$ is taken:

$$\begin{aligned} 0 &= \int \mathrm{d}\mathbf{x}\ \varphi_n^\dagger(\mathbf{x})\sum_k \left[\rho\ddot{q}_k\varphi_k(\mathbf{x}) + \rho\omega_k^2 q_k\varphi_k(\mathbf{x}) - m\delta(\mathbf{x}_\mathrm{p}-\mathbf{x})\omega_k^2 q_k\varphi_k(\mathbf{x}_\mathrm{p})\right] \\ &= A\rho\ddot{q}_n + A\rho\omega_n^2 q_n - m\varphi_n^\dagger(\mathbf{x}_\mathrm{p})\sum_k \omega_k^2 q_k\varphi_k(\mathbf{x}_\mathrm{p}). \end{aligned} \tag{4.9}$$

Here, $A = \pi R^2$ ($A = L$) for the membrane (beam) resonator; $A\rho = M$, the resonator mass. Equation (4.9) is divided by this M, and $\epsilon = m/M$ is defined.

After mode expansion, equation (4.6) becomes

$$m\ddot{\mathbf{x}}_\mathrm{p} - m\sum_k \omega_k^2 q_k\varphi_k(\mathbf{x}_\mathrm{p})\sum_\ell q_\ell\varphi_\ell'(\mathbf{x}_\mathrm{p}) = 0, \tag{4.10}$$

where $\varphi_\ell'(\mathbf{x}_\mathrm{p}) \equiv \nabla\varphi_\ell(\mathbf{x})|_{\mathbf{x}=\mathbf{x}_\mathrm{p}}$. Equation (4.10) is now extended to include the thermal diffusion of the particle across the resonator, by the insertion of a stochastic force $\sqrt{2m\gamma k_\mathrm{B}T}\xi(t)$ on the right-hand side and a friction term $m\gamma\dot{\mathbf{x}}_\mathrm{p}$ on the left-hand side. Finally, I take the overdamped limit, neglecting the inertial term $m\ddot{\mathbf{x}}_\mathrm{p}$, and divide through by $m\gamma$.

The final equations of motion for the system are thus

$$\begin{aligned} \ddot{q}_n + \omega_n^2 q_n - \epsilon\varphi_n^\dagger(\mathbf{x}_\mathrm{p})\sum_k \omega_k^2 q_k\varphi_k(\mathbf{x}_\mathrm{p}) &= 0, \\ \dot{\mathbf{x}}_\mathrm{p} - \frac{1}{\gamma}\sum_{k,\ell}\omega_k^2 q_k q_\ell\varphi_k(\mathbf{x}_\mathrm{p})\varphi_\ell'(\mathbf{x}_\mathrm{p}) &= \sqrt{2D}\ \xi(t), \\ \langle\xi(t)\rangle = 0, \quad \langle\xi(t)\xi(t')\rangle &= \delta(t-t'). \end{aligned} \tag{4.11}$$

For the rest of this chapter, the discussion is restricted to the beam resonator treated in Paper I [51], in which case $\mathbf{x}_\mathrm{p}$ becomes a scalar. The reason for this is that results for the membrane resonator are still forthcoming, due to the lack of existing algorithms for the numerical integration of stochastic differential

equations that include two uncorrelated stochastic forces.

4.2 Analytical solution – one vibrational mode

The full set of equations (4.11) are nonlinear and stochastic, and thus not possible to solve exactly. Instead, I will here study certain limiting cases. Only the fundamental vibrational mode will be included (the accuracy of this simplification is further discussed in section 4.3), and I separately examine the cases of large- and small-amplitude vibration.

The single-mode equations of motion are

$$\begin{aligned} \ddot{q}_0 + \omega_0^2 q_0 \left[1 - \epsilon\varphi_0^2(x_\mathrm{p})\right] &= 0 \\ \dot{x}_\mathrm{p} = \frac{\omega_0^2}{2\gamma}\partial_x[\varphi_0^2(x_\mathrm{p})] &+ \sqrt{2D}\,\xi(t). \end{aligned} \tag{4.12}$$

I make a change of variables into dimensionless action-angle variables $\mathcal{E}(\tau), \theta(\tau)$ by

$$\begin{aligned} \omega_0 t = \tau, \quad x_\mathrm{p}/L = \chi, \\ q_0(t) = L\sqrt{\mathcal{E}}\cos(\tau+\theta), \\ \dot{q}_0(t) = -\omega_0 L\sqrt{\mathcal{E}}\sin(\tau+\theta). \end{aligned} \tag{4.13}$$

Note that $\mathcal{E} \propto \dot{q}_0^2/\omega_0^2 L^2 \approx q_0^2/L^2$ Hence, $\mathcal{E}$ is proportional to the kinetic energy contained in the fundamental mode; it is henceforth referred to as the dimensionless mode energy. Later, in order to describe the mode energy of the n:th mode, I will use $\mathcal{E}_n \equiv \omega_n^2 q_n^2/\omega_0^2 L^2$.

The form of $\dot{q}_0$ leads to the condition $\dot{\mathcal{E}} = 2\mathcal{E}\dot{\theta}\tan(\tau+\theta)$, by means of which the transformed equations of motion are found to be

$$\begin{aligned} \partial_\tau \mathcal{E} &= -\epsilon\varphi_0^2 \mathcal{E}\sin 2(\tau+\theta), \\ \partial_\tau \theta &= -\epsilon\varphi_0^2\cos^2(\tau+\theta), \\ \partial_\tau \chi &= \frac{\omega_0}{2\gamma}\mathcal{E}\cos^2(\tau+\theta)\partial_\chi\varphi_0^2 + \sqrt{2\mathcal{D}}\xi(\tau), \end{aligned} \tag{4.14}$$

where $\mathcal{D} \equiv D/\omega_0 L^2$ is the dimensionless diffusion constant.

4.2.1 Large-amplitude vibrations

Particles adsorbed on a vibrating resonator will be driven towards and subsequently trapped near an antinode of vibration [29]. The fact that thermal fluctuations are now included in the model does not change this fact as long as the typical energy conferred to the adsorbate by the environment (the thermal energy) is much smaller than the kinetic energy of the particle due to the fact that it is moving together with the vibrating resonator. That is, if the

parameter

$$\frac{E_{\text{therm.}}}{E_{\text{vib.}}} = \frac{\frac{1}{2}k_{\text{B}}T}{\frac{1}{2}m\omega_0^2 q_0^2} = \frac{\gamma\mathcal{D}}{\omega_0\mathcal{E}} \tag{4.15}$$

is small, fluctuations in particle position are very small, and the phase noise can be neglected. In addition, since the particle position χ is almost constant, the nonlinear term can be expanded:

$$\partial_\chi\varphi_0^2(\chi) \approx \partial_\chi^2\varphi_0^2(\chi)|_{\chi=1/2}\ \chi = 2\varphi_0(\tfrac{1}{2})\varphi_0''(\tfrac{1}{2})\chi \equiv -k\chi. \tag{4.16}$$

I used that $\varphi_0'(\frac{1}{2}) = 0$ and dropped any constant terms. Using (4.16), the third of equations (4.14) can now be formally solved. It is equivalent to equation (3.2), but instead of a constant γ there is now an effective damping rate

$$\Gamma = \frac{\omega_0 k}{2\gamma}\mathcal{E}(\tau)\cos^2(\tau+\theta(\tau)). \tag{4.17}$$

The $\gamma(t-t')$ in the exponent of equation (3.3) is thus replaced by the integral of Γ from τ' to τ. That is ($\chi(\tau=0)=0$),

$$\chi(\tau) = \sqrt{2\mathcal{D}}\int_{-\infty}^{\tau} \mathrm{d}\tau'\xi(\tau')e^{-\frac{\omega_0 k}{2\gamma}\int_{\tau'}^{\tau}\mathrm{d}\tau''\mathcal{E}(\tau'')\cos^2(\tau''+\theta(\tau''))}. \tag{4.18}$$

To first non-vanishing order, $\varphi_0^2(\chi) \approx \frac{1}{2}k\chi^2$ (the expansion term linear in χ vanishes upon taking the average over the fluctuations $\xi(\tau)$). Using this together with equation (4.18), the first equation of (4.14) becomes

$$\begin{aligned}\partial_\tau\mathcal{E} \approx -\epsilon\mathcal{D}k\mathcal{E}(\tau)\sin 2(\tau+\theta)\int_{-\infty}^{\tau}\mathrm{d}\tau_1'\mathrm{d}\tau_2'\xi(\tau_1')\xi(\tau_2') \qquad (4.19)\\ \times\exp\left[-\frac{\omega_0 k}{2\gamma}\mathcal{E}(\tau)\left[\int_{\tau_1'}^{\tau}\mathrm{d}\tau''\cos^2(\tau''+\theta(\tau'')) + \int_{\tau_2'}^{\tau}\mathrm{d}\tau''\cos^2(\tau''+\theta(\tau''))\right]\right]\end{aligned}$$

where $\mathcal{E}(\tau)$ is assumed to be slowly varying compared to $\cos^2(\tau+\theta(\tau))$. For nanomechanical resonators this is generally the case, in particular for those manufactured of carbon. Such NEMS are characterized [40, 52] by high Q-factors, that measure the inverse decay of energy per period of oscillation, as well as high resonant frequencies, so that the period is very small. Taking the ensemble average of equation (4.19), $\langle\xi(\tau_1')\xi(\tau_2')\rangle = \delta(\tau_1'-\tau_2')$, which eliminates the $\mathrm{d}\tau_2'$-integral and makes the two integrals in the exponent equal. Finally, I average over one period in τ, causing the rapidly oscillating terms to vanish. The result is

$$\partial_\tau\mathcal{E} \approx 2\epsilon\mathcal{D}k\mathcal{E}(\tau)I\left(k\gamma^{-1}\omega_0\mathcal{E}(\tau)\right), \tag{4.20}$$

where the integral I is

$$I(z) = \frac{1}{2\pi}\int_0^{2\pi}\mathrm{d}\tau\sin 2\tau\int_{-\infty}^{\tau}\mathrm{d}\tau' e^{-z\int_{\tau'}^{\tau}\mathrm{d}\tau''\cos^2\tau''}, \tag{4.21}$$

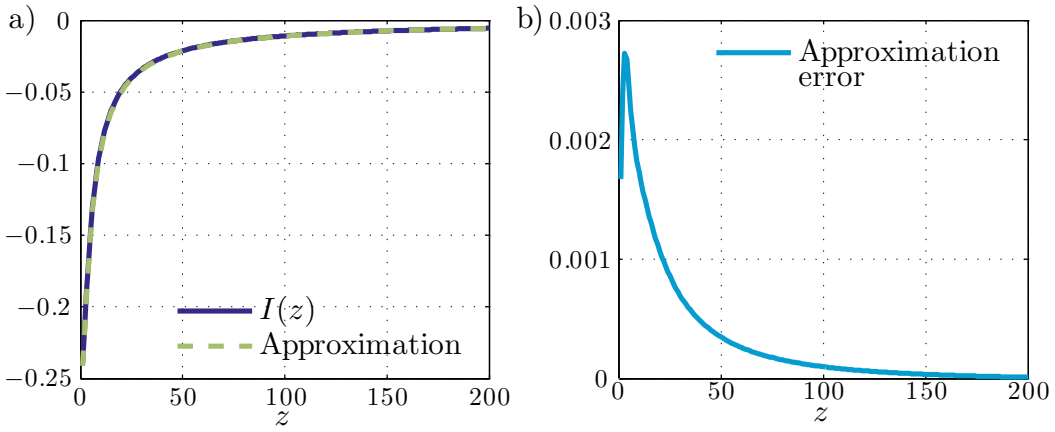

Figure 4.2: a) The integral (4.21) together with the approximation (4.22). b) The absolute value of the difference between the two curves in a).

$z \in \mathbb{R}$. As shown in figure 4.2, this integral is well approximated by

$$I(z) \approx -\left[4 + \sqrt{\pi}\left(\frac{z}{2}\coth\frac{z}{2} - 1\right)\right]^{-1}, \tag{4.22}$$

and the error of this approximation decreases as z increases. Since $\coth z \to 1$ when $z \to \infty$, for large vibrational amplitudes (corresponding to a large vibrational energy $\mathcal{E}$ and consequently a large z)

$$I(z) \approx -\left[4 + \sqrt{\pi}\left(\frac{z}{2} - 1\right)\right]^{-1} \approx -\frac{2}{\sqrt{\pi}z}. \tag{4.23}$$

Then, equation (4.21) becomes

$$\partial_\tau \mathcal{E} \approx -\epsilon\frac{4\mathcal{D}\gamma}{\omega_0\sqrt{\pi}}. \tag{4.24}$$

Hence, for resonator amplitudes that are large enough to inertially trap the particle, the vibrational energy of the resonator is expected to decay linearly.

4.2.2 Small-amplitude vibrations

If the resonator amplitude is small, one must assume that the particle is not inertially trapped but rather diffuses over the entire resonator surface. In order to analyse the system dynamics in this limit, the equivalent Fokker-Planck equation to the system (4.14) is found according to equation (3.7). Letting $\theta + \tau \equiv \nu$, a probability distribution $p(\mathcal{E}, \nu, \chi, \tau)$ is sought. I identify $\mathbf{x} = (\mathcal{E}, \nu, \chi)$,

and

$$\mathbf{A} = \begin{pmatrix} -\epsilon\varphi_0^2\mathcal{E}\sin 2\nu \\ 1-\epsilon\varphi_0^2\cos^2\nu \\ \frac{\omega_0}{2\gamma}\mathcal{E}\cos^2\nu\partial_\chi\varphi_0^2 \end{pmatrix}, \quad \mathbb{B} = \begin{pmatrix} 0 & 0 & 0 \\ 0 & 0 & 0 \\ 0 & 0 & \sqrt{2\mathcal{D}} \end{pmatrix}. \tag{4.25}$$

After some simplification, the corresponding FPE becomes

$$(\partial_\tau + \partial_\nu)p = \epsilon\varphi_0^2\left[\mathcal{E}\sin 2\nu\partial_\mathcal{E}p + \cos^2\nu\partial_\nu p\right] - \frac{\omega_0}{2\gamma}\mathcal{E}\cos^2\nu\partial_\chi(p\partial_\chi\varphi_0^2) + \mathcal{D}\partial_\chi^2 p. \tag{4.26}$$

As discussed in section 4.2.1, the vibrational energy $\mathcal{E}(\tau)$ is, in the case of nanomechanical resonators, a slowly varying function compared to the time scale ω_0^{-1}. This latter time scale is also characteristic of the particle diffusion, allowing for a separation of time scales in the FPE; the probability distribution is approximated as $p \approx p_0(\mathcal{E},\tau)p_1(\mathcal{E},\nu,\chi)$. Then, the particle position χ is completely described by the equation

$$\partial_\nu p_1 = -\frac{\omega_0}{4\gamma}\mathcal{E}(1+\cos 2\nu)\partial_\chi(p_1\partial_\chi\varphi_0^2) + \mathcal{D}\partial_\chi^2 p_1, \tag{4.27}$$

which can be solved using perturbation theory. That is, since $\gamma\mathcal{D}/\omega_0\mathcal{E} \gg 1$ (see equation (4.15) and discussion thereof), $\mathcal{E}$ must be small and the term proportional to it can be treated as a small correction to the one proportional to $\mathcal{D}$; the solution will be a power series $p_1 = p_1^{(0)} + \mathcal{E}p_1^{(1)} + \ldots$

To zeroth order in $\mathcal{E}$, equation (4.27) is $\partial_\nu p_1^{(0)} = \mathcal{D}\partial_\chi^2 p_1^{(0)}$. Since the vibrational energy in this limit is much smaller than the thermal energy, the sensible initial condition is that the particle is equally likely to be found anywhere along the resonator while $\mathcal{E} = \mathcal{E}_0$, the initial energy; $p_1^{(0)}(\mathcal{E},\nu=0,\chi) = \delta(\mathcal{E}-\mathcal{E}_0)$. Then, the zeroth order distribution is [46]

$$p_1^{(0)}(\mathcal{E},\nu,\chi) = \sum_n \cos n\pi\chi e^{-n^2\pi^2\mathcal{D}\nu}\int_0^1 \mathrm{d}\chi'\cos n\pi\chi' = 1, \tag{4.28}$$

since only the $n=0$-integral is nonvanishing.

To first order in $\mathcal{E}$, I find

$$\begin{aligned}\partial_\nu p_1^{(1)} - \mathcal{D}\partial_\chi^2 p_1^{(1)} &= -\frac{\omega_0}{4\gamma}\mathcal{E}(1+\cos 2\nu)\partial_\chi(p_1^{(0)}\partial_\chi\varphi_0^2) \\ &= -\frac{\omega_0}{4\gamma}\mathcal{E}(1+\cos 2\nu)\partial_\chi^2\varphi_0^2.\end{aligned} \tag{4.29}$$

This equation can be solved using separation of variables, where the χ-dependent part is again a Fourier cosine series, now with the initial condition $p_1^{(1)}(\mathcal{E},\nu=0,\chi) = \frac{\omega_0\mathcal{E}}{2\mathcal{D}\gamma}\varphi_0^2$. That is,

$$p_1^{(1)} = \frac{\omega_0\mathcal{E}}{2\gamma\mathcal{D}}\sum_n f_n N_n(\nu)\cos n\pi\chi. \tag{4.30}$$

where $f_n = \int_0^1 \mathrm{d}\chi' \varphi_0^2(\chi') \cos n\pi\chi'$.

By substituting (4.30) in (4.29) and taking the inner product with $\cos m\pi\chi$, I find that the function $N_n(\nu)$ is determined by the equation

$$N_n' + \lambda_n N_n = -\lambda_n(1 + \cos 2\nu), \quad \lambda_n = n^2\pi^2\mathcal{D}. \tag{4.31}$$

It is straight-forward to find that

$$N_n(\nu) = \lambda_n \frac{\lambda_n \cos 2\nu + 2\sin 2\nu}{\lambda_n^2 + 4} - 1. \tag{4.32}$$

The effect of the -1 will be to slightly change the constant value of the stationary solution $p_1^{(0)}$: a higher-order correction that may be neglected. Then, to first order in $\mathcal{E}$,

$$p_1(\mathcal{E}, \nu, \chi) = 1 + \frac{\omega_0 \mathcal{E}}{2\mathcal{D}\gamma} \sum_n \lambda_n f_n \frac{\lambda_n \cos 2\nu + 2\sin 2\nu}{\lambda_n^2 + 4} \cos n\pi\chi. \tag{4.33}$$

Returning to the full FPE (4.26), substituting the separable solution $p \approx p_0 p_1$ and using that p_1 solves (4.27), the equation becomes

$$\begin{aligned} p_1 \partial_\tau p_0 &= \epsilon\varphi_0^2 \left[\mathcal{E} \sin 2\nu (p_0 \partial_\mathcal{E} p_1 + p_1 \partial_\mathcal{E} p_0) + p_0 \cos^2\nu \partial_\nu p_1\right] \\ &= \epsilon\varphi_0^2 \Bigg[p_1 \mathcal{E} \sin 2\nu \partial_\mathcal{E} p_0 + \\ &\qquad p_0 \frac{\omega_0 \mathcal{E}}{\mathcal{D}\gamma} \sum_n \frac{f_n \lambda_n \cos n\pi\chi}{\lambda_n^2 + 4} \left[1 - \tfrac{1}{2}\lambda_n (1 + \cos 2\nu) \sin 2\nu\right] \Bigg]. \end{aligned} \tag{4.34}$$

Integrating over one period of the rapidly oscillating variable ν, I obtain

$$\partial_\tau p_0 = \varphi_0^2 \frac{\epsilon\omega_0}{2\mathcal{D}\gamma} \sum_n \frac{\lambda_n f_n \cos n\pi\chi}{\lambda_n^2 + 4} (\mathcal{E}^2 \partial_\mathcal{E} p_0 + 2 p_0 \mathcal{E}). \tag{4.35}$$

Finally, the fluctuations χ are integrated out, leaving the equation

$$\partial_\tau p_0 = \frac{\epsilon\omega_0}{2\mathcal{D}\gamma} \sum_n \frac{\lambda_n f_n^2}{\lambda_n^2 + 4} \partial_\mathcal{E} (\mathcal{E}^2 p_0) \tag{4.36}$$

that is solved by

$$p(\mathcal{E}, \tau) = \frac{1}{\mathcal{E}^2} f\left(\frac{1 - \alpha\mathcal{E}\tau}{\mathcal{E}}\right), \quad \alpha = \frac{\epsilon\omega_0}{2\mathcal{D}\gamma} \sum_n \frac{\lambda_n f_n^2}{\lambda_n^2 + 4} \tag{4.37}$$

for some function f. However, the initial condition $p(\mathcal{E}, \tau = 0) = \delta(\mathcal{E} - \mathcal{E}_0)$ requires that $f(\mathcal{E}^{-1}) = \mathcal{E}^2 \delta(\mathcal{E} - \mathcal{E}_0)$, which determines the exact shape of f.

Thus, I conclude that

$$p(\mathcal{E},\tau) = \frac{1}{\mathcal{E}^2}\frac{\mathcal{E}^2}{(1-\alpha\mathcal{E}\tau)^2}\delta\left(\frac{\mathcal{E}}{1-\alpha\mathcal{E}\tau} - \mathcal{E}_0\right) = \frac{1}{(1-\alpha\mathcal{E}\tau)^2}\delta\left(\mathcal{E} - \frac{\mathcal{E}_0}{1+\alpha\mathcal{E}_0\tau}\right). \tag{4.38}$$

Then, the time evolution of the average energy is

$$\langle\mathcal{E}(\tau)\rangle = \int \mathrm{d}\mathcal{E}'\,\mathcal{E}'p(\mathcal{E}',\tau) = \int \mathrm{d}\mathcal{E}'\frac{\mathcal{E}'}{(1-\alpha\mathcal{E}'\tau)^2}\delta\left(\mathcal{E}' - \frac{\mathcal{E}_0}{1+\alpha\mathcal{E}_0\tau}\right) = \frac{\mathcal{E}_0}{1+\alpha\mathcal{E}_0\tau}, \tag{4.39}$$

a decay that is characteristic of a nonlinearly damped oscillator.

The decay (4.39) tends to zero, and not to the $k_\mathrm{B}T$ given by the equipartition of energy. This error is amended by a more formal treatment that also includes fluctuation corrections; see Appendix B of Paper I for details.

4.3 Numerical solution – N vibrational modes

The preceding analytical analysis has shown the following:

i) for resonator amplitudes that are large enough to inertially trap the adsorbate, the vibrational energy is expected to decay linearly,

ii) for small resonator amplitudes, when the particle is free to diffuse across the entire resonator, the energy is expected to decay in the manner of a nonlinearly damped resonator.

However, the analysis of section 4.2 was done in a single mode-framework, where the displacement field $w(x,t) = q_0(t)\varphi_0(x)$. Clearly, then, it must be verified to what degree these results are valid as excited vibrational modes are included.

To study the full dynamics of the system, I numerically integrate the system of equations (4.11) using a second order algorithm [53]. The chosen initial condition is that all vibrational energy in the system is in the fundamental mode, a condition that is easy to achieve experimentally by choosing the corresponding actuation frequency. The particle is chosen to be initially adsorbed at the center of the resonator – at the antinode of φ_0. This is an experimentally realistic choice as long as the initial resonator amplitude is large; simulations confirm that the relocation of the particle from any starting position to the inertially trapped position is very rapid. The chosen nanotube dimensions are shown in table 4.1.

Working with the dimensionless quantities defined in section 4.2, I choose $\mathcal{D} = 2.85\times10^{-4}, \gamma = 0.241\omega_0$ and $\epsilon = 1.82\times10^{-2}$. This ϵ corresponds to the mass m of a mid-sized protein or a larger collection of non-interacting smaller nanoparticles. The simulation temperature is set to 500 K and the initial vibrational energy of the fundamental mode is $\mathcal{E}_0(\tau=0) = 0.044 \simeq 10^4 k_\mathrm{B}T$ (recall that $\mathcal{E}_n(\tau) = \omega_n^2 q_n^2(\tau)/\omega_0^2 L^2$). This is simultaneously a large adsorbate mass,

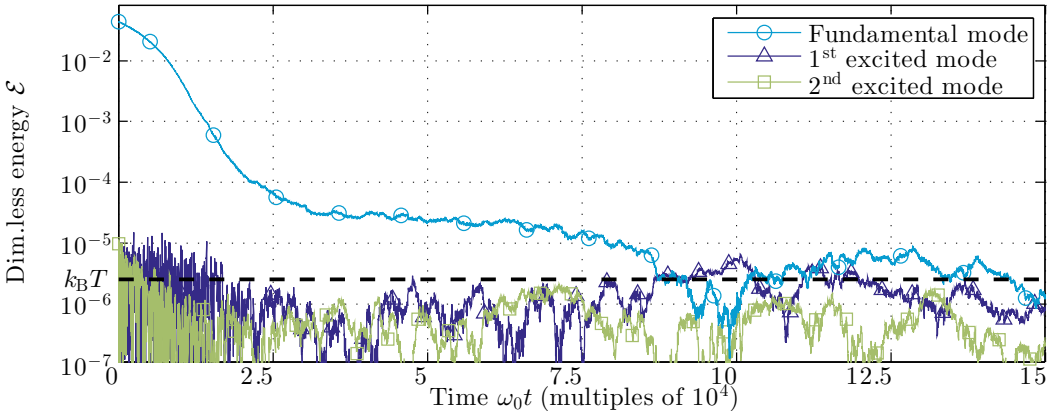

Figure 4.3: Dimensionless mode energies as function of time during ring-down of the fundamental mode, shown in a logarithmic scale. For clarity, only the lowest lying flexural modes are shown; higher modes behave similarily. The dashed line indicates the thermal energy in dimensionless units.

Table 4.1: Resonator dimensions used in the simulations. The mass of the nanotube is $M = \pi d L \rho_G$, where $\rho_G = 760$ ag/μm^2 is the graphene mass density.

Length	L	1 μm
Diameter	d	5 nm
Mass	M	12 ag
Fundamental frequency	ω_0	$2\pi \times 108$ MHz

high intial amplitude, high simulation temperature, and strong interaction between particle and substrate (determined by γ). These parameter values have been chosen to be reasonably realistic, while still allowing for numerical stability and clear visualization of the found diffusion-induced effects. If nothing else is stated, these are the values used in all subsequent calculations.

Figure 4.3 shows the vibrational energy contained in the three lowest lying modes during a simulated ring-down experiment. The mode coupling mediated by the adsorbed particle is clearly evident; $\mathcal{E}_1(0) = \mathcal{E}_2(0) = 0$, but the excited modes seem to have thermalized almost instantly. As the simulation progresses, the diffusing particle acts to damp out the fundamental mode and establish equilibrium with higher-lying modes. The same data is shown in linear scale in figure 4.4 a), together with a fit clearly showing that the fundamental mode energy decays linearly. In figure 4.4 b) I show the evolution of the probability distribution for the particle position. The high- and low-amplitude regimes are clearly separated, as indicated by the dashed line; the particle is initially trapped near the antinode (where $\chi = 1/2$) while the vibrational amplitude is high, and diffuses freely when the amplitude has decayed.

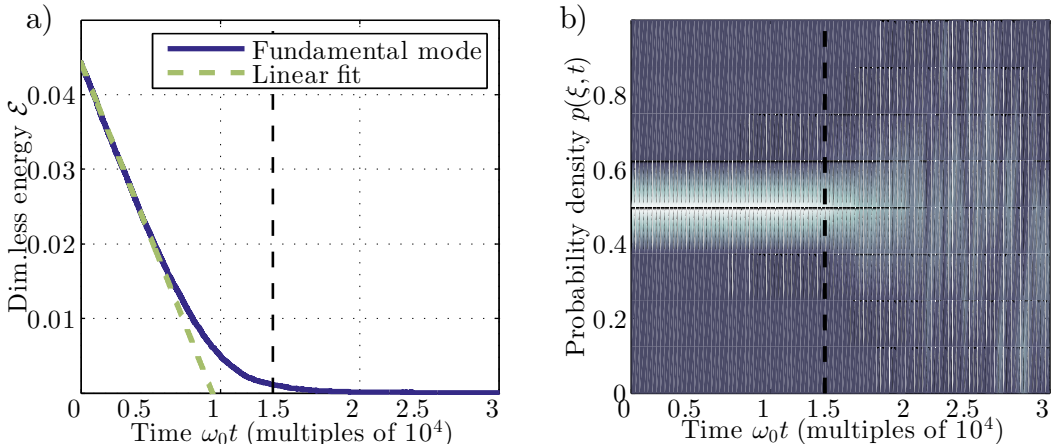

Figure 4.4: Illustration of the transition between the high-amplitude regime, where the adsorbate is inertially trapped at the vibration antinode, and the low-amplitude regime, where the thermal fluctuations overcome the inertial trapping potential and the particle diffuses freely. The horizontal dashed line approximately indicates the point where the dynamics changes from one regime to the other. In a), the vibrational energy $\mathcal{E}$ of the fundamental mode is shown together with a linear fit to the initial decay. In b) is shown the evolution of the probability distribution $p(\chi, t)$, where $\chi = x_\mathrm{p}/L$. Early during the ringdown, there is a very high probability to find the particle near the antinode at $\chi = 1/2$, but as time progresses and the amplitude decreases, $p(\chi, t)$ becomes nearly uniform.

To more closely investigate the nature of the mode coupling, I use that $\mathcal{E}_{n>0} \ll \mathcal{E}_0$ initially. Thus, for times $\tau \gtrsim 0$ and $n > 0$, the first equation in (4.11) becomes

$$\ddot{q}_n + \omega_n^2 q_n \approx \epsilon \omega_0^2 q_0 \varphi_0(x_\mathrm{p}) \varphi_n(x_\mathrm{p}). \tag{4.40}$$

Making a change to action-angle variables $(\mathcal{E}_n(\tau), \theta_n(\tau))$, defined in analogy with equation (4.13), leads to $\partial_\tau \mathcal{E}_n \propto \epsilon q_0 \sin(\omega_n t + \theta_n)$. Since $q_0 \propto \sqrt{\mathcal{E}_0}$, a first approximation of the mode energy is

$$\langle \mathcal{E}_n \rangle \propto \epsilon^2 \mathcal{E}_0(0) \tau, \quad n > 0. \tag{4.41}$$

In order to test this relation, I define the thermalization time τ_therm as the time when $\mathcal{E}_n$ first exceeds $k_\mathrm{B}T$ for *some* $n > 0$; τ_therm is thus a lower bound for the time taken for *all* excited modes to reach thermal equilibrium. The thermalization time for a wide range of adsorbate masses and initial amplitudes were found from integration of equation (4.11); the resulting values for τ_therm are shown in figure 4.5. The data was fitted to a model $\tau_\mathrm{therm} \propto (\epsilon^a \mathcal{E}_0(0))^{-b}$, where the sum of squared residuals was found to be minimized by $a = 1.86, b = 1.24$. This is quite reasonable agreement with the theoretical values of $a = 2, b = 1$ considering the roughness of the approximation (4.41) and that τ_therm by construction underestimates actual time required for thermalization.

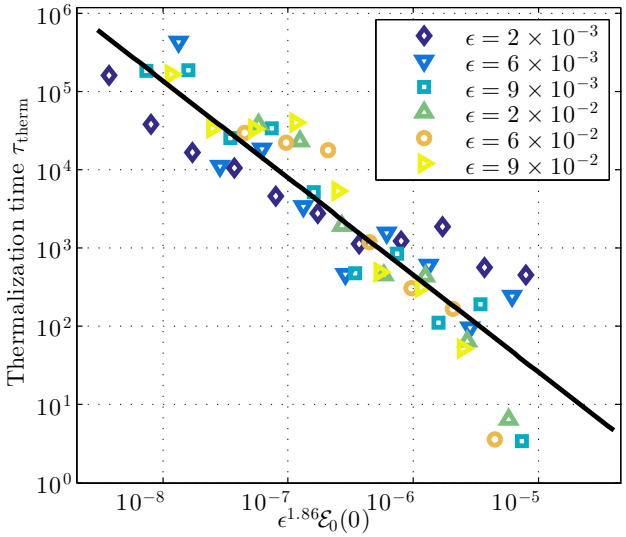

Figure 4.5: Dependence of the thermalization time on ϵ and $\mathcal{E}_0(0)$. The black line is a least-squares fit to the data. The numerical simulation becomes more sensitive the more energy is put into the system, which explains the increased spread of the data points as $\mathcal{E}_0(0)$ increases

The mode coupling due to the particle is thus explained to a high degree by the adsorbate simply being present, with no dependence on the fact that it diffuses. However, that the particle changes position ensures that, eventually, all modes do couple to each other and hence thermalize. In the calculation of figure 4.3, $\chi(0) = 1/2$ which means that $\phi_1(\chi(0)) = 0$. The first excited mode would thus have remained frozen out for the duration of the simulation, were it not for the (initially small) fluctuations of χ around the starting position of the particle.

In light of the discussion above, it is clear that the excited modes can be assumed to be in thermal equilibrium on the time scale relevant for the resonator ring-down from an initial amplitude $\mathcal{E}_0(0) \gg k_{\mathrm{B}}T$. The collection of excited modes then function as a background thermal bath, and the single mode-results of section 4.2 are thus qualitatively correct. It is not surprising, then, to realize that the mechanism behind the damping of the fundamental mode seen in figure 4.3 is actually present already in the single mode-regime.

If χ (and hence $\varphi_0^2(\chi)$) does *not* contain a frequency component $\sin 2\nu$, integrating the $\mathcal{E}$-equation in (4.14) over rapid oscillations will lead to $\partial_\tau \mathcal{E} = 0$. Since it is quite clear in figure 4.3 that $\partial_\tau \mathcal{E} \neq 0$, χ must contain such a frequency component just as $\mathcal{E}$ does: the two variables are correlated. In other words, the particle motion is not independent from the resonator motion. Physically, this correlation manifests in that the effect of the kicks from the particle on the nanotube does not average to zero, as one might have expected given white noise diffusion. Instead, the kicks will counter the resonator motion more often

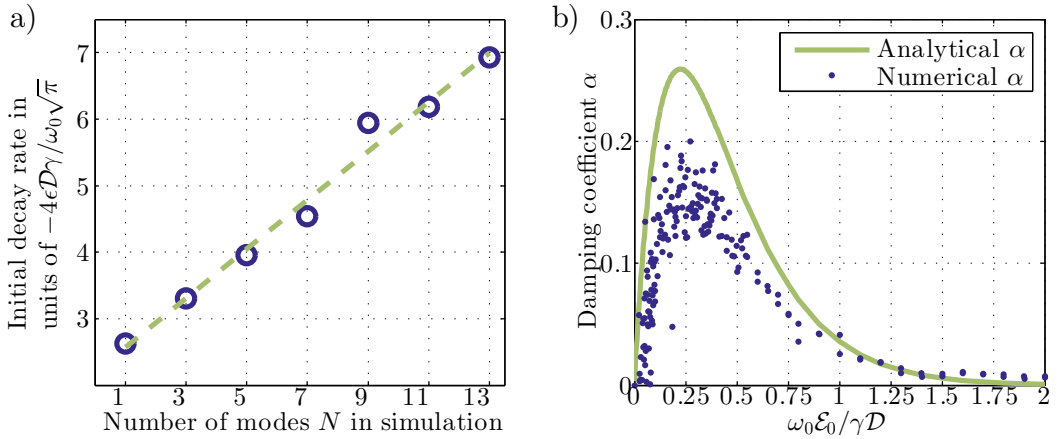

Figure 4.6: a) Slope of the decay of the fundamental mode during the initial, linear regime, as a function of the number of modes N included in the simulation; circles are data points while the dashed line is a linear fit. b) Damping parameter α, as calculated by equation (4.37) (solid line) and by a numerical fit (dots).

than they amplify it, resulting in a net damping.

It is not only the fundamental mode that is subject to dissipation induced by the diffusing particle; such dissipation is the reason why the higher modes only gain energy until they thermalize around $k_{\mathrm{B}}T$. The mode coupling does not, however, cease to act; vibrational energy is continually transferred from the fundamental mode to the higher-lying modes, and subsequently dissipated by the stochastic force caused by the adsorbate. Hence, once thermalized, each excited mode acts as a new dissipation channel for the fundamental mode; a result analogous to those of [26,27] where conservative geometric nonlinearities were introduced in clean nanoresonators. The dependence of the decay rate on N, the number of modes included in the simulation, is shown in figure 4.6 a). The decay rate of $\mathcal{E}_0$ is expressed in units of $-4\epsilon\mathcal{D}\gamma/\omega_0\sqrt{\pi}$ in order to facilitate comparision with the analytical result (4.24).

In principle, $N \to \infty$, so there must be some cutoff at which including more excited modes does not translate into a higher decay rate. I have not determined this cut-off numerically, since the fact that the mode frequencies increase quadratically with n (see table 2.1) means that the time step used in the integration quickly becomes unmanageably small when N increases. Instead, the cut-off is analytically estimated by noting that the typical distance covered by the diffusing particle during one period of the fundamental mode is $\sqrt{4\pi D/\omega_0}$. If this distance is larger than half the wave length λ_n, the coupling between the n:th mode and the fundamental mode will average to zero. Since $\lambda_n = 2L/(n+1)$, the cutoff condition is given by

$$\frac{2L}{n+1} = \sqrt{\frac{4\pi D}{\omega_0}} = 2L\sqrt{\pi\mathcal{D}}, \tag{4.42}$$

so only modes with $n \lesssim n_{\max} \approx (\pi\mathcal{D})^{-1/2}$ will contribute as extra dissipation channels. For the value of $\mathcal{D}$ used in figure 4.6 a), $n_{\max} \simeq 20$.

Finally, in order to test the validity of the perturbative calculation in section 4.2.2, the computed energy evolution was fitted to a curve of the shape (4.39), and the parameter α was extracted. The initial energy was set to $\mathcal{E}_0(0) = 10^{-4}$, and the ratio $\omega_0\mathcal{E}_0/\gamma\mathcal{D}$ (the inverse of equation (4.15)) was varied by changing the simulation temperature. All other simulation parameters were the same as those used in figure 4.3. This numerically determined α is shown together with the analytical curve (4.37) in figure 4.6 b). It is evident that the perturbative approach is indeed valid for $\omega_0\mathcal{E}_0/\gamma\mathcal{D} \ll 1$, and while (4.37) overestimates the magnitude of the damping in the intermediate region $\omega_0\mathcal{E}_0/\gamma\mathcal{D} \lesssim 1$, the qualitative behaviour of α is captured.

5 Summary and outlook

I have studied the interaction of a linear mechanical resonator and a particle adsorbed on and allowed to diffuse over its surface. In the nonlinear coupling of two of the paradigm systems of physics – an harmonic oscillator in the shape of a resonator vibrational mode, and a random walker – surprisingly complex dynamics arise. The main result of this thesis is the investigation of two new mechanisms of dissipation in a carbon nanotube nanomechanical resonator, mechanisms induced by the diffusing particle.

First, the adsorbed particle mediates a mode coupling between the vibrational modes of the resonator. By means of this coupling, vibrational energy is transferred from the initially excited fundamental mode to intially frozen excited modes, causing the latter to rapidly reach thermal equilibrium. Once equilibrized, each excited mode functions as a dissipation channel, that siphons energy from the fundamental mode and dissipates it to the environment, via the friction between the resonator and the adsorbate.

Second, the motion of the resonator and the adsorbate, respectively, are not independent processes. The existence of correlations between the oscillation and the diffusion means that the effect of the stochastic force on the resonator does not average to zero, as one might expect from a white noise process. Instead the force creates a net nonexponential damping. Two regimes are identified; when the vibration amplitude of the resonator is large, the adsorbate is inertially trapped at an antinode of the vibration, and the mode energy decays linearly. When the vibration amplitude is small, on the other hand, the thermal fluctuations overcome the inertial trapping, and the particle diffuses over the entire resonator; the fundamental mode energy then decays in a manner characteristic of a nonlinearly damped resonator.

In the future, I aim to finish my work on diffusing a adsorbates on graphene resonator, partially discussed in this thesis. Since the systems are quite similar, the two novel dissipation mechanisms found in the case of carbon nanotube resonators are expected to be present in graphene resonators as well; a prediction that seems to be confirmed by preliminary simulations. There is, however, one qualitative difference between the systems; a two-dimensional graphene resonator will have a large number of degenerate eigenmodes. The adsorbation of a stationary particle breaks this degeneracy, but what will happen if the particle is allowed to diffuse? I look forward to investigating this problem further.

In general, the results of this thesis need experimental verification. While, for example, the thermalization rate depend only on adsorbate mass, device geometry, and initial amplitude – parameters that are easily accessible in experiments – it is not clear in what manner the found dissipation mechanisms interact with other mechanisms, or if the found dissipation rates will be possible to isolate and measure.

The applicability of the results presented in this thesis is not limited only to mass sensing measurements, where particles are intentionally deposited on a resonator. In any kind of experiment that takes place outside of vaccum, there is a chance that air molecules or heavier particles, for example pollen grains, will attach to a resonator, and confound the results. To better reflect such a situation, my model can be extended to include several diffusing particles, as well as to allow for adsorbtion- and desorbtion-events.

Finally, one complication that I have here ignored is the nonlinear nature of carbon nanoresonators. The inclusion of, say, a Duffing nonlinearity in the equations of motion would be an interesting extension of the present model.

Acknowledgements

There are many friends, family members, and colleagues without whom my work, my writing, and my sanity would be have been far more lacking; none mentioned and none forgotten. However, a few people do deserve a special mention:
My supervisor, Andreas Isacsson, for productive discussions of terrible algebra.
My parents, Lennart and Sonja Edblom, for unceasing faith and support, to the point of driving a trailer with all my belongings from Umeå to Gothenburg at an average speed of 72 km/h.
My dear fiancé, Tobias Rhén, for always ruining things with reason.

I gratefully acknowledge financial support from the Foundation for Strategic Research (SSF), as well as the European Union through Grant No. 246026 and the GRAPHENE Flagship.

Bibliography

[1] G. E. Moore. Cramming more components onto integrated circuits. *Electronics*, 38, 1965.

[2] A. N. Cleland and M. L. Roukes. A nanometre-scale mechanical electrometer. *Nature*, 392:160, Mar 1998.

[3] G. A. Steele, A. K. Hüttel, B. Witkamp, M. Poot, H. B. Meerwaldt, L. P. Kouwenhoven, and H. S. J. van der Zant. Strong coupling between single-electron tunneling and nanomechanical motion. *Science*, 325:1103, Aug 2009.

[4] H. J. Mamin and D. Rugar. Sub-attonewton force detection at millikelvin temperatures. *Applied Physics Letters*, 79:3358, 2001.

[5] R. G. Knobel and A. N. Cleland. Nanometre-scale displacement sensing using a single electron transistor. *Nature*, 424:291, Jul 2003.

[6] M. D. LaHaye, O. Buu, B. Camarota, and K. C. Schwab. Approaching the quantum limit of a nanomechanical resonator. *Science*, 304:74, 2004.

[7] D. Rugar, R. Budakian, H. J. Mamin, and B. W. Chui. Single spin detection by magnetic resonance force microscopy. *Nature*, 430:329, Jul 2004.

[8] K. L. Ekinci, Y. T. Yang, and M. L. Roukes. Ultimate limits to inertial mass sensing based upon nanoelectromechanical systems. *Journal of Applied Physics*, 95:2682, Feb 2004.

[9] K. Jensen, K. Kim, and A. Zettl. An atomic-resolution nanomechanical mass sensor. *Nature Nanotechnology*, 3:533, Sep 2008.

[10] B. Lassagne, D. Garcia-Sanchez, A. Aguasca, and A. Bachtold. Ultrasensitive mass sensing with a nanotube electromechanical resonator. *Nano Letters*, 8:3735, 2008.

[11] J .L. Arlett, E. B. Myers, and M. L. Roukes. Comparative advantages of mechanical biosensors. *Nature Nanotechnology*, 6:203, Apr 2011.

[12] J. Chaste, A. Eichler, J. Moser, G. Ceballos, R. Rurali, and A. Bachtold. A nanomechanical mass sensor with yoctogram resolution. *Nature Nanotechnology*, 7:301, May 2012.

[13] M. S. Hanay, S. Kelber, A. K. Naik, D. Chi, S. Hentz, E. C. Bullard, E. Colinet, L. Duraffourg, and M. L. Roukes. Single-protein nanomechanical mass spectrometry in real time. *Nature Nanotechnology*, 7:602, Sep 2012.

[14] Paul A. M. Dirac. *The Principles of Quantum Mechanics*. Oxford University Press, fourth edition, 1958.

[15] K. Eom, H. S. Park, D. S. Yoon, and T. Kwon. Nanomechanical resonators and their applications in biological/chemical detection: Nanomechanics principles. *Physics Reports*, 503:115, 2011.

[16] A. N. Cleland and M. L. Roukes. Noise processes in nanomechanical resonators. *Journal of Applied Physics*, 92:2758, Sep 2002.

[17] M. I. Dykman, M. Khasin, J. Portman, and S. W. Shaw. Spectrum of an oscillator with jumping frequency and the interference of partial susceptibilities. *Phys. Rev. Lett.*, 105:230601, Dec 2010.

[18] J. Atalaya, A. Isacsson, and M. I. Dykman. Diffusion-induced dephasing in nanomechanical resonators. *Phys. Rev. B*, 83:045419, Jan 2011.

[19] Y. T. Yang, C. Callegari, X. L. Feng, and M. L. Roukes. Surface adsorbate fluctuations and noise in nanoelectromechanical systems. *Nano Letters*, 11:1753, 2011.

[20] J. Atalaya. Mass loading induced dephasing in nanomechanical resonators. *Journal of Physics: Condensed Matter*, 24:475301, 2012.

[21] R. Lifshitz and M. L. Roukes. Thermoelastic damping in micro- and nanomechanical systems. *Phys. Rev. B*, 61:5600, Feb 2000.

[22] M. C. Cross and R. Lifshitz. Elastic wave transmission at an abrupt junction in a thin plate with application to heat transport and vibrations in mesoscopic systems. *Phys. Rev. B*, 64:085324, Aug 2001.

[23] I. Wilson-Rae. Intrinsic dissipation in nanomechanical resonators due to phonon tunneling. *Phys. Rev. B*, 77:245418, Jun 2008.

[24] A. Eichler, J. Moser, J. Chaste, M. Zdrojek, I. Wilson-Rae, and A. Bachtold. Nonlinear damping in mechanical resonators made from carbon nanotubes and graphene. *Nature Nanotechnology*, 6:339, Jun 2011.

[25] A. Croy, D. Midtvedt, A. Isacsson, and J. M. Kinaret. Nonlinear damping in graphene resonators. *Phys. Rev. B*, 86:235435, Dec 2012.

[26] D. Midtvedt, A. Croy, A. Isacsson, Z. Qi, and H. S. Park. Fermi-Pasta-Ulam physics with nanomechanical graphene resonators: Intrinsic relaxation and thermalization from flexural mode coupling. *Phys. Rev. Lett.*, 112:145503, Apr 2014.

[27] A. W. Barnard, V. Sazonova, A. M. van der Zande, and P. L. McEuen. Fluctuation broadening in carbon nanotube resonators. *Proceedings of the National Academy of Sciences*, 109:19093, 2012.

[28] J. Atalaya. Nanomechanical mass measurement using nonlinear response of a graphene membrane. *Europhysics Letters*, 91:48001, Sep 2010.

[29] J. Atalaya, A. Isacsson, and M. I. Dykman. Diffusion-induced bistability of driven nanomechanical resonators. *Phys. Rev. Lett.*, 106:227202, May 2011.

[30] H. B. Meerwaldt, S. R. Johnston, H. S. J. van der Zant, and G. A. Steele. Submicrosecond-timescale readout of carbon nanotube mechanical motion. *Applied Physics Letters*, 103:053121, 2013.

[31] R. van Leeuwen, A. Castellanos-Gomez, G. A. Steele, H. S. J. van der Zant, and W. J. Venstra. Time-domain response of atomically thin mos2 nanomechanical resonators. *Applied Physics Letters*, 105:041911, 2014.

[32] L. D. Landau and E. M. Lifshitz. *Mechanics*, volume 1 of *Course of Theoretical Physics*. Butterworth-Heinemann, third edition, 1981.

[33] L. D. Landau and E. M. Lifshitz. *Theory of Elasticity*, volume 7 of *Course of Theoretical Physics*. Butterworth-Heinemann, third edition, 1986.

[34] J. S. Bunch, A. M. van der Zande, S. S. Verbridge, I. W. Frank, D. M. Tanenbaum, J. M. Parpia, H. G. Craighead, and P. L. McEuen. Electromechanical resonators from graphene sheets. *Science*, 315:490, Aug 2007.

[35] D. Garcia-Sanchez, A. M. van der Zande, A. San Paulo, B. Lassagne, P. L. McEuen, and A. Bachtold. Imaging mechanical vibrations in suspended graphene sheets. *Nano Letters*, 8:1399, Apr 2008.

[36] C. Chen, S. Rosenblatt, K. I. Bolotin, W. Kalb, P. Kim, I. Kymissis, H. L. Stormer, T. F. Heinz, and J. Hone. Performance of monolayer graphene nanomechanical resonators with electrical readout. *Nature Nanotechnology*, 4:861, Sep 2009.

[37] A. M. Eriksson, D. Midtvedt, A. Croy, and A. Isacsson. Frequency tuning, nonlinearities and mode coupling in circular mechanical graphene resonators. *Nanotechnology*, 24:395702, Sep 2013.

[38] V. Sazonova, Y. Yaish, H. Ustunel, D. Roundy, T. A. Arias, and P. L. McEuen. A tunable carbon nanotube electromechanical oscillator. *Nature*, 431:284, Sep 2004.

[39] D. Garcia-Sanchez, A. San Paulo, M. J. Esplandiu, F. Perez-Murano, L. Forró, A. Aguasca, and A. Bachtold. Mechanical detection of carbon nanotube resonator vibrations. *Phys. Rev. Lett.*, 99:085501, Aug 2007.

[40] A. K. Hüttel, G. A. Steele, B. Witkamp, M. Poot, L. P. Kouwenhoven, and H. S. J. van der Zant. Carbon nanotubes as ultrahigh quality factor mechanical resonators. *Nano Letters*, 9:2547, Mar 2009.

[41] B. Lassagne, Y. Tarakanov, J. Kinaret, D. Garcia-Sanchez, and A. Bachtold. Coupling mechanics to charge transport in carbon nanotube mechanical resonators. *Science*, 325:1107, Aug 2009.

[42] J. Atalaya, A. Isacsson, and J. M. Kinaret. Continuum elastic modeling of graphene resonators. *Nano Letters*, 8:4196, Oct 2008.

[43] Karl F. Graff. *Wave Motion in Elastic Solids*. Dover Publications, Inc., 1975.

[44] M. I. Katsnelson and A. Fasolino. Graphene as a prototype crystalline membrane. *Accounts of Chemical Research*, 46:97, Oct 2013.

[45] N. Lindahl, D. Midtvedt, J. Svensson, O. A. Nerushev, N. Lindvall, A. Isacsson, and E. E. B. Campbell. Determination of the bending rigidity of graphene via electrostatic actuation of buckled membranes. *Nano Letters*, 12:3526, Jun 2012.

[46] Gerald B. Folland. *Fourier Analysis and Its Applications*. American Mathematical Society, 1992.

[47] C. W. Gardiner. *Handbook of Stochastic Methods for Physics, Chemistry and the Natural Sciences*. Springer, second edition, 1985.

[48] A. O. Caldeira and A. J. Leggett. Influence of dissipation on quantum tunneling in macroscopic systems. *Phys. Rev. Lett.*, 46:211, Jan 1981.

[49] Daniel Midtvedt. *Nonlinear electromechanics of nanomembranes and nanotubes*. PhD thesis, Chalmers University of Technology, 2013.

[50] P. Langevin. Sur la théorie du mouvement brownien. *C. R. Acad. Sci.*, 146:530, 1908.

[51] C. Edblom and A. Isacsson. Diffusion-induced dissipation and mode coupling in nanomechanical resonators. *Phys. Rev. B*, 90:155425, Oct 2014.

[52] K. L. Ekinci and M. L. Roukes. Nanoelectromechanical systems. *Review of Scientific Instruments*, 76:061101, May 2005.

[53] R. Mannella and V. Palleschi. Fast and precise algorithm for computer simulation of stochastic differential equations. *Phys. Rev. A*, 40:3381, Sep 1989.

Paper I